ELSEVIER

Journal of Nuclear Materials 294 (2001) 274–287

journal of nuclear materials

www.elsevier.nl/locate/jnucmat

The role of Cu in displacement cascades examined by molecular dynamics

C.S. Becquart [a,*], C. Domain [b], J.C. van Duysen [a,b], J.M. Raulot [b,1]

[a] *Laboratoire de Métallurgie Physique et Génie des Matériaux, UMR 8517, Bât. C6, Université Lille I, F-59655 Villeneuve d'Ascq cedex, France*

[b] *EDF – DRD Département EMA, Les renardières, F-77818 Moret sur Loing cedex, France*

Received 27 September 2000; accepted 17 January 2001

Abstract

Molecular dynamics simulations of displacement cascades in pure Fe, Fe–0.2 at.% Cu and Fe–2 at.% Cu have been done with different primary knocked-on atom (PKA) energies. The typical defects (vacancies and interstitials) appear during the cascade process. Most of the defects recombine in the first few picoseconds. The presence of Cu atoms does not seem to influence the primary damage in the time span covered by MD. Neither Cu precipitates, nor dilute atmospheres have been observed to form in the course of the MD simulations. However, a tendency to form mixed objects (vacancies or interstitials gathered with Cu atoms) is noticed in the Fe–2 at.% Cu. Our feeling is that the numerous vacancies left at the end of the cascade recombination phase will interact with the Cu atoms and will act as attractive centers. The role of the interstitials is less clear for the moment.

PACS: 82.20.WT; 34.20.CF

1. Introduction

The pressure vessels of light water reactors are made with low alloyed steels. While in service, the neutron irradiation decreases the fracture toughness of these steels. The power utilities employ several procedures to determine the state of the vessel and to confirm that the safety margins against brutal rupture are preserved. While the reliability of these procedures are well established, studies are still in progress to improve upon them. Particularly, there is an international effort to identify the nature of the damage induced by neutrons in ferritic steels [1–5].

It is now well known that copper atoms play an important role in this damage. Microstructural studies have revealed at least two types of neutron-irradiation induced defects involving copper in low Cu content alloys (Cu content lower than 0.2%). One defect type is the *dilute cluster* (sometimes called an atmosphere). As its name implies, it is a localized region where solute atoms gather together in higher concentrations than in the bulk alloy, but the region is still predominantly Fe. Dilute clusters of solute atoms (Cu, Ni, Si, Mn) have been observed by the tomographic atom probe [6,7].

The second defect type is the copper–vacancy complex, which is approximately four vacancies bound to one copper atom [6,8].

Some uncertainties still remain about the origin, structure and stability of these defects. Their mechanisms of interaction with dislocations as well as their behavior during annealing treatments also need to be

* Corresponding author. Tel.: +33-3 20 43 69 27; fax: +33-3 20 43 40 40.

E-mail addresses: charlotte.becquart@univ-lille1.fr (C.S. Becquart), christophe.domain@edf.fr (C. Domain), jean-claude.van-duysen@edf.fr (J.C. van Duysen), raulot@spms.ecp.fr (J.M. Raulot).

[1] Present address: Ecole Centrale Paris, Laboratoire Structures, Propriétés et Modélisations, des Solides, grande voie des vignes, 92295 Chatenay Malabry, France.

0022-3115/01/$ - see front matter
PII: S0022-3115(01)00421-4

clarified. Recent experimental studies have suggested answers to some of these issues [4–6,8]. In order to confirm and to complement these answers, we have undertaken a study to characterize the effects of irradiation in Fe–Cu binary alloys by numerical simulations (molecular dynamics and Monte Carlo).

We performed MD simulations of displacement cascades at different temperatures, with different energies in pure Fe with one potential chosen from the literature in [9] and in Fe–Cu dilute random solid solution with the Fe–Cu potential [10] built from the previously mentioned Fe potential. Two concentrations were examined: a low Cu content: Fe–0.2 at.% Cu and a high Cu content: Fe–2 at.% Cu to emphasize the Cu atoms effect on the cascades. Displacement cascades are initiated when an atom in the solid, the primary knocked-on atom (PKA) receives an energy higher than a few hundred eV. Their development can be roughly divided into three phases: the collision phase, lasting $\sim 10^{-13}$ s, during which the PKA energy is shared among successive generations of recoil atoms, a relaxation period, which lasts less than a picosecond during which defects begin to adopt their equilibrium configurations and a cooling phase which lasts a few picoseconds during which the highly disordered cascade volume reaches local thermal equilibrium with the surrounding lattice. The cooling rates and the temperature gradients are very high ($>10^{15}$ K/s and $>10^{12}$ K m^{-1}, respectively). The lifetime of a cascade is therefore in the range of a few picoseconds, its size, a few nanometers; this makes displacement cascades ideal subjects for MD studies in pure metals, see for instance [11–14], as well as in alloys, see for instance [15–17]. Current MD simulations have now covered most of the neutron energy spectrum relevant to fission reactors, and for reviews of the simulation of displacement cascades in metals and alloys see for instance [18–20]. The primary damage created by the recoil atoms has been described very thoroughly in these review articles. Calder et al. [21] studied the effect of displacement cascades in both a dilute (1 at.% Cu) random solid solution of Cu and small coherent precipitates in an α-Fe matrix. They observed that cascades caused only small changes to the distribution of Cu atoms and that vacancies tended to bind to Cu atoms.

This work, which objective is to analyze the role of Cu atoms on the primary damage, is part of the REVE project. The paper is organized as follows:

In a first part, we briefly present the computer code and outline the computational procedure for displacement cascade simulations.

We then examine the interatomic potential used in this work, concentrating on the basic properties of the Fe–Cu potential and compare them with two other potentials available in literature [22–25]. A more detailed characterization of the α-Fe component of the potential (analytical formula, elastic constants, defect energies, thermal properties and threshold displacement energies) can be found in [26], where the influence of the cohesive models was examined using three different α-Fe potentials. In the discussion section, we compare the damage obtained in pure α-Fe to that obtained in Fe–0.2 at.% Cu (concentration at which the solute atmospheres are observed to form under neutron irradiation experiments) as well as in Fe–2 at.% Cu alloys (concentration at which precipitates form under neutron irradiation experiments). For our purpose, the damage is characterized by the number of residual defects (vacancies), the cascade volume determined by component analysis and the tendency to make clusters (number and size of the clusters) of defects. We focus mostly on the vacancies, as the data scattering for the interstitials is too important to be able to extract any trend. We then conclude.

2. Computational procedure

2.1. The DYMOKA code

The code we use, DYMOKA, is a modified version of CDCMD: a user oriented code developed at the University of Connecticut by Rifkin to do Monte Carlo and MD simulations (a version in C-programming language is available in [27]). It has been parallelized by message passing using MPI and vectorized by Domain [28]. The newtonian equations of motion are integrated using a fifth-order Gear predictor–corrector algorithm. The neighbor search is done through a link cell method combined with a Verlet list so that the code is fully linear with the number of atoms. The interatomic potentials are tabulated and interpolation of the potentials is made through a fifth-order Lagrange polynomial.

An energy minimization method algorithm called quench molecular dynamics (QMD) derived after [29,30] is also included in DYMOKA. It is used to calculate defect energies. A post processing code (PHO) was written for defects detection, and calculation of pair distribution functions $g(r)$, local temperatures, cluster distributions etc.

2.2. MD cascades simulations

To simulate displacement cascades some approximations were made:

Following many author's scheme [31,32], the effect of electron–phonon coupling has been ignored.

The boundary atoms were not damped to extract heat or attenuate the out-going pressure wave. According to Phythian et al. [19], the temperature dependence of the residual defects and of the defect clustering fraction is weak. This has been confirmed by Gao et al. [33] who investigated the problem very thoroughly.

Table 1
Number of displacement cascades for each PKA energy

	5 (keV)	10 (keV)	20 (keV)
Fe	6	6	6
Fe–0.2 at.% Cu	5	6	6
Fe–2 at.% Cu	–	4	6

At the beginning of the simulation, the system of particles is let to equilibrate, for 5 ps, at the chosen temperature, 600 K, to be close to the vessel irradiation temperature. When the lattice is at thermal equilibrium, one atom, the PKA is given a momentum corresponding to energies varying from 1 to 30 keV. The actual time step varies from 10^{-17} s (at the beginning of the collision phase) to 10^{-15} s.

The choice of the simulation box size depends upon the energy of the PKA. It must be large enough to avoid the displacement cascade to interfere with itself by periodic overlap. This point is checked visually and a posteriori. Our simulations were done in the microcanonical ensemble with periodic boundary conditions.

Variability was introduced by changing the initial distribution of the velocities, the random distribution of the Cu atoms (in the solid solution) and the PKA direction. These directions ($\langle 1\,3\,5\rangle$ and $\langle 2\,5\,3\rangle$) were chosen to be representative of an average behavior.

Table 1 displays the number of simulations done in each case.

2.3. Damage characterization

To distinguish between the crystallographic point defects (vacancies and interstitials), different characterizations are possible. In this work, we used the scheme developed by Vascon [34] which allows the identification of vacancies, true or single interstitials, dumbbells and replaced atoms. In what follows, for simplicity, we will not distinguish between the different interstitial types: 'true interstitials', dumbbells I and dumbbells II.

The amount of incascade clustering is important since small clusters can be very mobile and provide easy nucleation sites for larger defects to grow. As divacancies tend to be in second nearest-neighbor position (see Table 6), we define a vacancy cluster as a configuration in which each vacancy has at least one second nearest-neighbor position occupied by a vacancy. For the interstitials, the two defects have to be within the nearest-neighbor distance to belong to the same cluster.

To characterize the cascade expansion, we use component analysis. Component analysis is an efficient technique to uniquely associate to each individual displacement cascade, an ellipsoid which accounts for its spatial extension and its morphology on the basis of its intrinsic characteristics [35]. The information provided by this method is the direction of three orthogonal axes that are associated to the spatial point defect distribution and the variance of this distribution projected onto them. The major axis has the direction maximising the variance, the second maximises the variance of the distribution projected onto a plane perpendicular to the first and the third one has the direction minimising this variance. These directions are parallel to the directions of the eigenvectors of the covariance matrix of the point defect distributions and the associated eigenvalues are the variances of the distribution projected onto the directions of the eigenvectors. These ellipsoids define what we will call the cascade cores. In what follows, and for simplicity, each core volume will be considered as representative of one displacement cascade. Similarly, the anisotropy of each cascade core can be measured as the ratio between the lengths of the axes maximising and minimising the projected distribution variances.

3. The interatomic potentials

The potentials used in this work were built according to the embedded atom method (EAM) [36] by Ludwig et al. [10]. They were adapted to the simulation of cascades by Raulot [37]. In the following section, we present the equilibrium properties of the potentials. In the next section, we present the cascade oriented properties. The hardening procedure can be found in Appendix A.

3.1. The interatomic potentials: equilibrium properties

3.1.1. The Fe potential

There exist many EAM-like potentials to model the properties of α-Fe, and Ludwig et al. [10] used the interatomic potential given by Simonelli et al. [9]. This potential has already been used for other purposes, see for instance [38]. In Table 2, we summarize its main characteristics; more properties can be found in [26] (potential Fe III). We refer the reader to the original article [9] for more details on the parameterization.

3.1.2. The Cu potential

For Cu, Ludwig et al. [10] used the interatomic potential given by Voter [47]. As this potential was derived for the fcc phase, we present below the behaviour of the bcc phase. We refer the reader to the original article [47] for more details on the parameterization.

3.1.2.1. bcc Cu lattice parameter. In Table 3 is presented a comparison of the lattice parameter of bcc Cu with the lattice parameter of α-Fe for the potential used in this work as well as for the two other Fe–Cu potentials.

All the potentials predict that the lattice parameter of α-Fe is smaller than that of bcc Cu and that a small Cu precipitate should induce compressive stresses in the lattice as observed by Phythian [49]. However, the

Table 2
Equilibrium lattice constant, cohesive energy, elastic constants, vacancy formation energy, vacancy migration energy, interstitial formation energies, threshold displacement energies

	This work	Experimental
Typical data fitted upon		
a_0 (Å)	2.8664	2.87[a]
E_{coh} (eV)	4.28	4.28[a]
$C_{11} \times 10^{11}$ Pa	2.42	2.43[b], 2.33[c], 2.37[d]
$C_{12} \times 10^{11}$ Pa	1.47	1.38[b], 1.35[c], 1.41[d]
$C_{44} \times 10^{11}$ Pa	1.1	1.22[b], 1.18[c], 1.16[d]
$C' \times 10^{11}$ Pa	0.48	0.53[b], 0.49[c], 0.48[d]
B(10^{11} Pa)	1.79	1.68[a]
Vacancy properties		
E^f_{vac} (eV)	1.63	≈2[e], 1.53[f]
E^m_{vac} (eV)	0.66	0.55[g,h], 1.28[f]
Interstitial formation energies		
$E_{dumbbell\langle 1\,1\,1\rangle}$ (eV)	Becomes crowdion	–
$E_{dumbbell\langle 1\,1\,0\rangle}$(eV)	3.67	–
$E_{dumbbell\langle 1\,0\,0\rangle}$ (eV)	4.57	–
$E_{crowdion}$ (eV)	3.54	–

[a] Ref. [39].
[b] Ref. [40].
[c] Ref. [41].
[d] Ref. [42].
[e] Ref. [43].
[f] Ref. [44].
[g] Ref. [45].
[h] Ref. [46].

magnitude of the stresses is much higher for the potential derived by Ackland than for the two other potentials.

3.1.2.2. Energy and volume differences between the bcc and fcc structures for Cu. In Table 4, some values found in the literature for fcc–bcc energy and volume differences at 0 K for Cu are compared with those predicted by the potential used in this work. The ab initio values can strongly differ according to the authors. Our EAM-based values fall in the same range of magnitude.

3.1.3. The Fe–Cu potential

Ludwig et al. [10] adjusted the Fe–Cu interaction on the vacancy–Cu binding energy in the α-Fe matrix, to the energy of solution of one Cu atom in the α-Fe matrix and to the kinetic binding energy between two Cu atoms. We here also refer the reader to the original article [10] for more details on the parameterization.

In this section, we present some important properties of the Fe–Cu interaction, and when possible, a comparison is made with two other Fe–Cu potentials found in literature:

The potential derived by Ackland et al. [25].
The potential derived by Osetsky et al. [22–24].

3.1.3.1. Partial molar energy of Cu at infinite dilution. The cohesive energy for an AB alloy can be approximated using the following equation:

$$E^{A-c\%B}_{coh} = cE^B_{coh} + (1-c)E^A_{coh} + \Delta E^c_m,$$

where c is the B content, and E^A_{coh} and E^B_{coh} are the cohesive energies of pure A and pure B, respectively and ΔE^c_m is the mixing energy. For a regular solution, ΔE^c_m is given by $\Delta E^c_m = \Omega c(1-c)$, where Ω is an energy parameter (corresponding to the partial molar energy of B at infinite dilution or the heat of solution). The partial molar energy of Cu at infinite dilution for the potential used in this work is given in Table 5 and compared to experimental values and the value obtained by Ackland et al. [25]. The experimental values are quite scattered as they are computed from Cu solubility limits which are not very precisely known and themselves very scattered specially at low temperatures.

3.1.3.2. Lattice parameter vs %Cu. We determined the evolution of the lattice parameter (at 0 K) of the Fe–Cu solution vs the copper content by finding, for each temperature, the lattice parameter canceling the stress and/or minimizing the energy (see Fig. 1). For each composition, the copper atoms were randomly placed in the lattice. The comparison to experiments and to Ackland's potential can be seen in Fig. 1. The potential used in this work tends to overestimate the lattice dilation with Cu content.

3.1.3.3. Binding energies. The binding energies between two entities in a bcc iron matrix were calculated as follows. The binding energy E^{A-B}_b of an A–B pair (Cu–Cu, Cu–vacancy or vacancy–vacancy) is defined as the dif-

Table 3
bcc Cu lattice parameter compared to the α-Fe lattice parameter for three Fe–Cu potentials[a]

This work (Å)			Ackland[b] (Å)			Osetsky[c] (Å)			Ab initio[d] (Å)
bcc Cu	α-Fe	ΔV (%)	bcc Cu	α-Fe	ΔV (%)	bcc Cu	α-Fe	ΔV (%)	bcc Cu
2.88	2.866	0.015	2.9607	2.8665	0.11	2.885	2.867	0.019	2.892

[a] ΔV is the volume difference between α-Fe and bcc Cu.
[b] Ref. [25].
[c] Ref. [23].
[d] Ref. [48].

Table 4
Energy and volume difference between the bcc and fcc structures for Cu

		$E_{fcc} - E_{bcc}$ (meV)	$(\Omega_{fcc} - \Omega_{bcc})/\Omega_{fcc}$ (%)
Ab initio	Kraft et al.[a]	7	−4.3
	Lu et al.[b]	49	−0.8
	Becquart et al.[c]	37	−0.43
Semi-empirical potentials	Ackland et al.[d]	24	−9.9
	Osetsky et al.[e]	–	−1.7
	This work	46	−1.21

[a] Ref. [50].
[b] Ref. [51].
[c] Ref. [48].
[d] Ref. [25].
[e] Ref. [23].

Table 5
Partial molar energy of Cu at infinite dilution (heat of solution)

This work (eV)	Fe–Cu Ackland[a] (eV)	Experimental (eV)
0.497	0.317	0.317[a] 0.49[b] 0.59[c]

[a] Ref. [25].
[b] Ref. [52].
[c] Ref. [53].

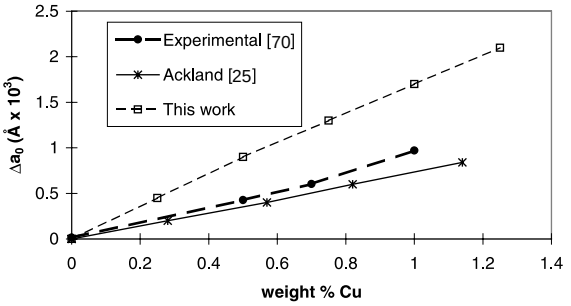

Fig. 1. Lattice parameter evolution vs Cu content [25,70].

ference of the two system energies E_1 and E_2, system 1 where A and B do not interact, i.e., the distance between A and B is greater than the potential cut-off, and system 2 where A and B interact. The distance between A and B may be first nearest neighbor distance, second nearest neighbor distance and so on. The binding energy E_b^{A-B} is the difference between the two total system energies, $E_b^{A-B} = E_1 - E_2$.

The relaxed binding energies calculated with this procedure are given in Table 6 which also presents the values obtained with the two other published Fe–Cu potentials.

The most stable relaxed configurations are the first nearest neighbors for the Cu–Cu system and Cu–V system and the second nearest neighbors for the vacancy–vacancy system in agreement with the two other potentials. The magnitude of the energies differ but the tendency is the same.

Table 6
Relaxed binding energies in the α-Fe matrix: vacancy–vacancy, vacancy–Cu, Cu–Cu[a]

	This work (eV)	Ackland[b] (eV)	Osetsky[c] (eV)
V–V 1nn	0.16	0.14	−0.02
V–V 2nn	0.21	0.19	0.20
Cu– V 1nn	0.19	0.087	0.14
Cu–V 2nn	−0.03	0.04	0.02
Cu–Cu 1nn	0.2	0.075	0.20
Cu–Cu 2nn	−0.02	0.035	0.08

[a] 1nn = first nearest neighbor distance, 2nn = second nearest neighbor distance.
[b] Ref. [25].
[c] Ref. [23,24].

To our knowledge, the only experimental value published for the Cu–vacancy binding energy is 0.14 eV [54]. The relative positions of the Cu atom and the vacancy are unknown, it is thus difficult to compare to our results. Masuda [55] investigated the properties of vacancy-type lattice defects in bcc transition metals using a tight binding type electronic theory. His results show that the most stable relaxed configuration for the divacancy in transition metals is when the vacancies are second nearest neighbors. This is also observed experi-

Table 7
Kinetic binding energies

	This work (eV)	Ackland[a] (eV)	Osetsky[b] (eV)
$E_b^k(2)$	0.01	−0.012	0.06

[a] Ref. [25].
[b] Ref. [23,24].

mentally [56,57] in Mo and is indeed the case with our model.

The kinetic binding energy is given by: $E_b^k(2) \approx E_b^{Cu-Cu} - E_b^{V-Cu}$ and the obtained values are summarized in Table 7. In their model of precipitate growth kinetics, Golubov et al. [58] found that the kinetic binding energy $E_b^k(2)$ should not exceed about 0.05 eV so that small Cu precipitates could dissociate thermally. Consequently, Osetsky and Serra [24] adjusted their potentials on this value.

It is to be mentioned at this point that the 0 K binding energies of vacancies and of Cu atoms are not sufficient data to determine if vacancy clusters are more stable than Cu atom clusters. For instance, the temperature has to be taken into account (at low-temperatures, voids are frequently observed, while at higher temperatures, the main defects are Cu-rich dilute clusters [59]). One must also consider the influence of interfacial energy as well as the role of other species on the growth of precipitates [60]. Interfacial energy will have an effect on small precipitates stability and when they reach the critical size to grow. Consequently, it is a priori very difficult to say what will be the stable defects after the simulation of displacement cascades from a consideration of the binding energies only, but these data can give some insight on the potentials behavior.

3.2. The interatomic potentials: cascade oriented properties

3.2.1. Threshold displacement energies

The threshold displacement energy is the minimum kinetic energy transmitted to one atom to create a stable Frenkel pair (a vacancy and an interstitial). It is an important parameter in radiation damage theory. It depends on the materials and on the orientation of the primary recoil.

The threshold displacement energies have been calculated when the recoil atom is a single substitutional copper atom in an Fe matrix and compared to these of pure Fe (values in parenthesis). The results are collected in Table 8 along with the experimental data available for α-Fe [61]. There exists no experimental data for the threshold displacement energies for a Cu atom in an α-Fe matrix and for the potentials studied here, the fact that the recoil atom is a Cu atom seems to have only a very small influence.

Table 8
Threshold displacement energies for a Cu atom in an α-Fe matrix[a]

PKA direction	This work (eV)	Fe–Cu Ackland[b] (eV)	Experimental α-Fe[c] (eV)
⟨1 0 0⟩	18 ± 1 (17 ± 1)	≈19 (≈20)	17
⟨1 0 0⟩	>30 (30 ± 1)	>100 (>100)	>30
⟨1 1 1⟩	19 ± 1 (20 ± 1)	≈32 (≈30)	20

[a] The values in parenthesis are the threshold displacement energies for pure Fe.
[b] Ref. [25].
[c] Ref. [61].

4. Results

The overall damage picture is similar to what can be found in the literature, see for instance [13,20,26]: the cascade generates numerous defects; vacancies are mostly located near the core of the cascade while interstitials can be found mostly in the periphery. Some of the defects form small clusters while the others remain isolated.

One point worth mentioning here is the data scattering as was emphasized in [26]. Even at high PKA energies, where one would expect the cascades to become more 'typical' and the fluctuations to become smaller as observed by Stoller [62], large fluctuations can be observed. Despite these, the residual defects distribution functions are narrow, this was already studied by several authors either analytically [63] or on the basis of BCA calculations in [64], and a fair estimate (with a reasonable standard error) of the mean number of residual defects can be obtained using only 8–10 cascades at 10 and 20 keV [62]. For computational time limits, we were not able to reach that kind of accuracy for all the PKA and the Cu content studied, nevertheless, we feel that the statistics we have been able to reach are sufficient for our purpose. Furthermore, other cascades characteristics distributions (the tendency to form clusters, the cascade shape, ...) are not as narrow as the number of residual defects, and the means exhibit large error bars.

4.1. Residual damage

4.1.1. Cascades shapes and sizes

Fig. 2 presents the typical aspect of a 20 keV cascade in pure Fe and a 20 keV cascade in Fe–0.2 at.% Cu. Both cascades look very similar. There are some dense areas which are onsets of subcascades and a fair amount of replacement collision sequences (RCS). The recoil energies of an Fe atom or a Cu atom are very similar (Table 8) and the presence of a few Cu atoms in the Fe matrix does not change the overall aspect of the cascades.

The extension of the cascade affected zone can be assessed, for instance, by the number of atoms which do

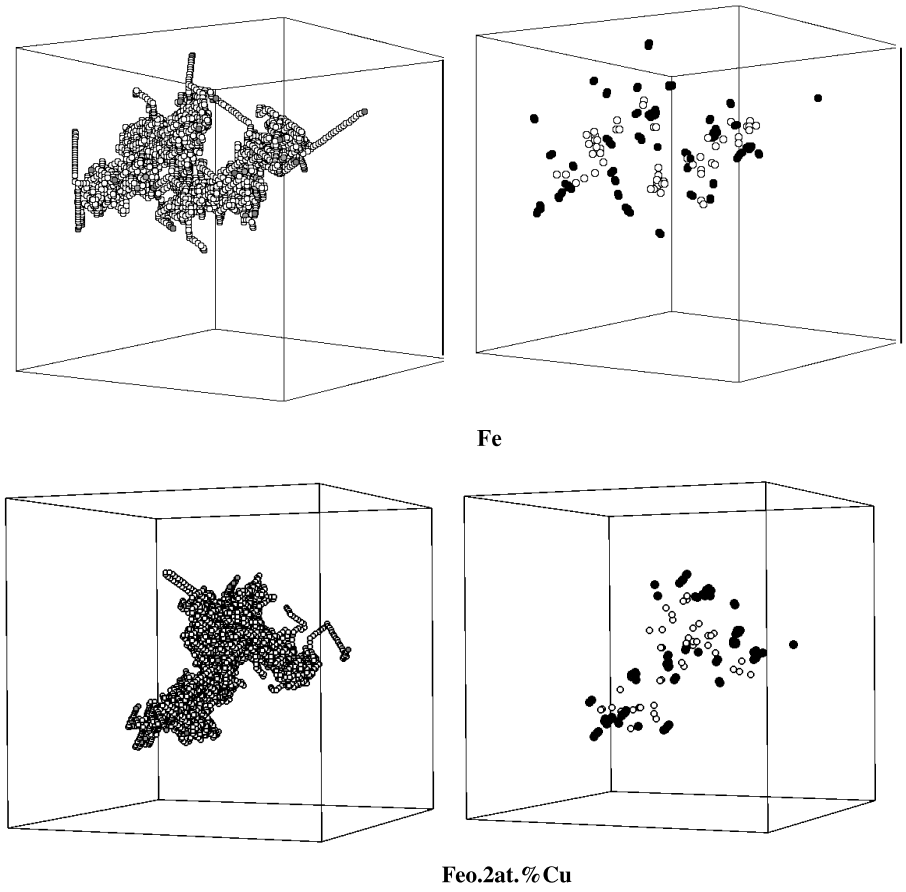

Fig. 2. Typical aspect of a 20 keV cascade at 600 K for α-Fe and Fe–0.2 at.% Cu at the end of the recombination phase. Left-hand side: the big empty circles are the replaced atoms, the big dark circles are the interstitials. Right-hand side the dark circles are interstitials, the empty ones are vacancies. Box' size 23 nm.

not lie on their original site (replaced atoms) at the end of the cascade. This number gives a measure of the atomic mixing which in the case of a pure element has no importance, but does play a role in alloys, specially in ordered ones. In Fig. 3 appear averaged histograms of the distances traveled by all the replaced atoms for pure Fe, Fe–0.2 at.% Cu and Fe–2 at.% Cu for 10 and 20 keV PKA. No significant differences can be observed between pure Fe and the dilute Cu alloys, this is not really surprising as the atomic masses of iron and copper are

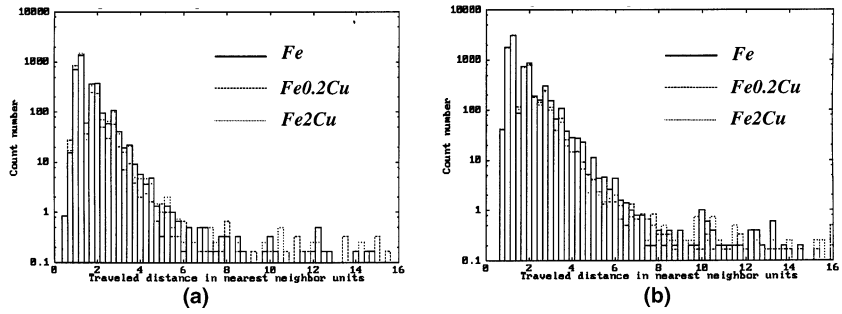

Fig. 3. Distance traveled by replaced atoms histograms in units of nearest neighbor distance in Fe and dilute Fe–Cu alloys at 600 K: (a) $E_p = 10$ keV; (b) $E_p = 20$ keV.

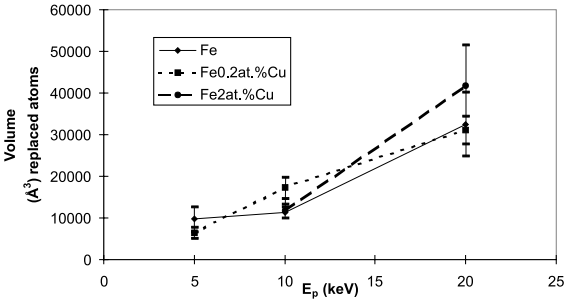

Fig. 4. Cascade size as determined from the replaced atoms in Fe and dilute Fe–Cu alloys vs PKA energy at 600 K.

very close and long displacements are caused by the collision phase of the cascade.

Another way of estimating the 'damage extension' is to use component analysis on the residual defects to define a cascade volume. Fig. 4 presents the evolution of the cascade volume estimated on the vacancies remaining at the end of the cascades for three PKA energies. The higher the PKA energy, the larger the cascade radius, therefore the more important the atomic mixing (more atoms leave their original lattice positions), but no difference again can be seen between the cascades done in pure Fe and those done in the dilute Cu alloys.

4.1.2. Residual damage

The number of residual vacancies (the results here are not given relative to the NRT prediction) increases with the PKA energy (Fig. 5) as is typically observed in displacement cascade simulations. The number of residual defects follows the power law proposed by Bacon, $N = AE_{\mathrm{p}}^{B}$ with $A = 5.0$ and $B = 0.74$ for pure Fe and $A = 4.6$ and $B = 0.76$ for Fe–0.2 at.% Cu values which compare well with Bacon et al.'s values $A = 5.57$ and $B = 0.83$ for pure Fe [65].

It appears that the presence of Cu atoms does not seem to change the amount of residual vacancies. One can notice that the standard error is much smaller for the number of residual defects than for the cascade shape.

The tendency of the isolated defects created by the cascades to gather and form clusters is a very important part of the damage picture one tries to obtain from the simulations. Indeed, small glissile loops would not have the same impact on the mechanical properties as large sessile clusters. For the 20 keV cascades, approximately 30% of the residual vacancies form clusters. The fluctuations in the number of vacancy clusters are important, and it is therefore difficult to find any trends with the PKA energy as can be seen in Fig. 6. The error band is also quite important, however, in that aspect too, it appears that the presence of Cu atoms does not seem to have any noticeable influence. The vacancy clusters are small: they contain up to five vacancies only (Fig. 7(a)–(c)).

The data scattering is even more important for the interstitial clusters [26] and it is even more difficult to find any trend in the results. The number of interstitials gathered in clusters is a little bit higher than the vacancies in clusters as it seems closer to 40%. The interstitial cluster sizes are also more important (they contain up to 17 interstitials for the 2 at.% Cu alloy), and the presence of Cu atoms does not seem to have any noticeable influence as can be seen in Fig. 8(a)–(c).

From the above results, it appears that the Cu atoms do not play any noticeable role in the displacement cascade simulations as no obvious differences in the cascades morphology, in the residual damage and on the defects spatial distribution were found.

To investigate the problem more thoroughly, we have examined the number of residual defects close to Cu atoms. Table 9 presents the number of V–Cu and I–Cu pairs observed at the cascade end. These numbers are compared to what would have been obtained if the Cu atoms had been distributed at random in an array containing the residual vacancies (resp. interstitials) formed during the cascade (the so called 'random pairs'

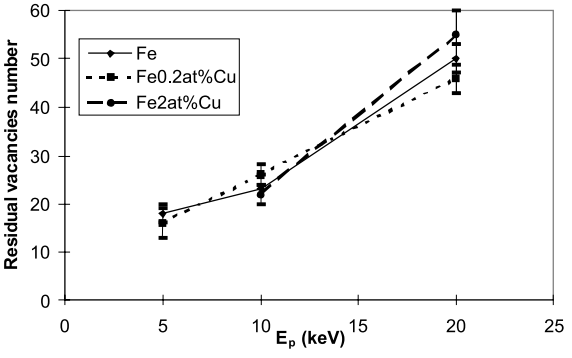

Fig. 5. Average number of residual vacancies in Fe and dilute Fe–Cu alloys vs PKA energy at 600 K.

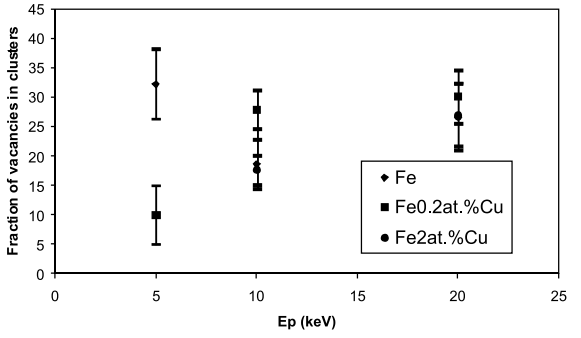

Fig. 6. Amount of vacancies in clusters in Fe and dilute Fe–Cu alloys vs PKA energy at 600 K.

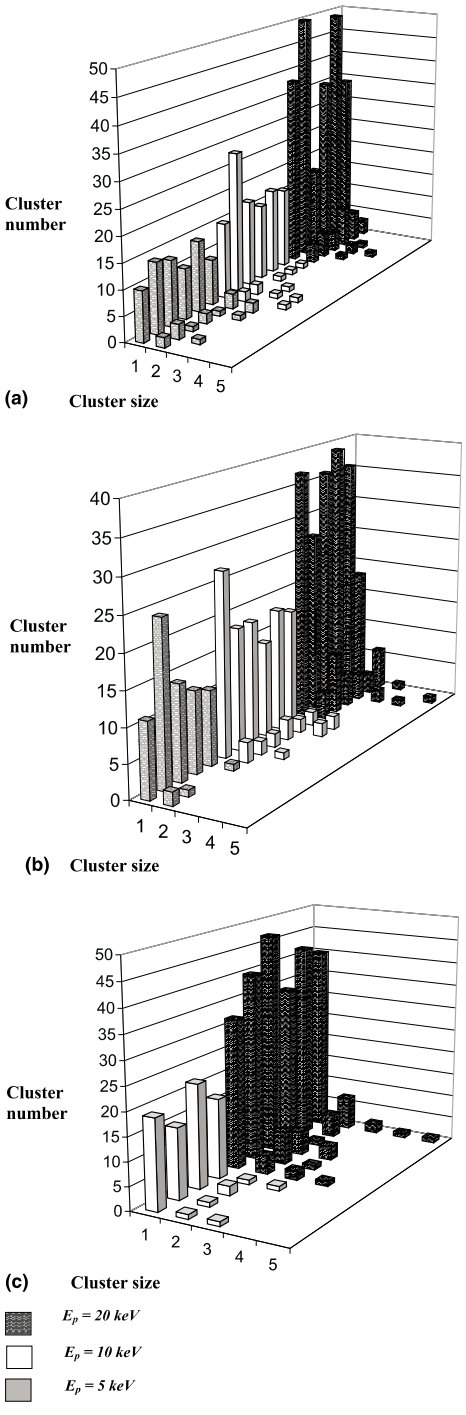

Fig. 7. Size of vacancy clusters in Fe (a), Fe–0.2 at.% Cu (b) and Fe–2 at.% Cu (c) vs PKA energy at 600 K. ■ $E_p = 20$ keV; □ $E_p = 10$ keV; ▨ $E_p = 5$ keV.

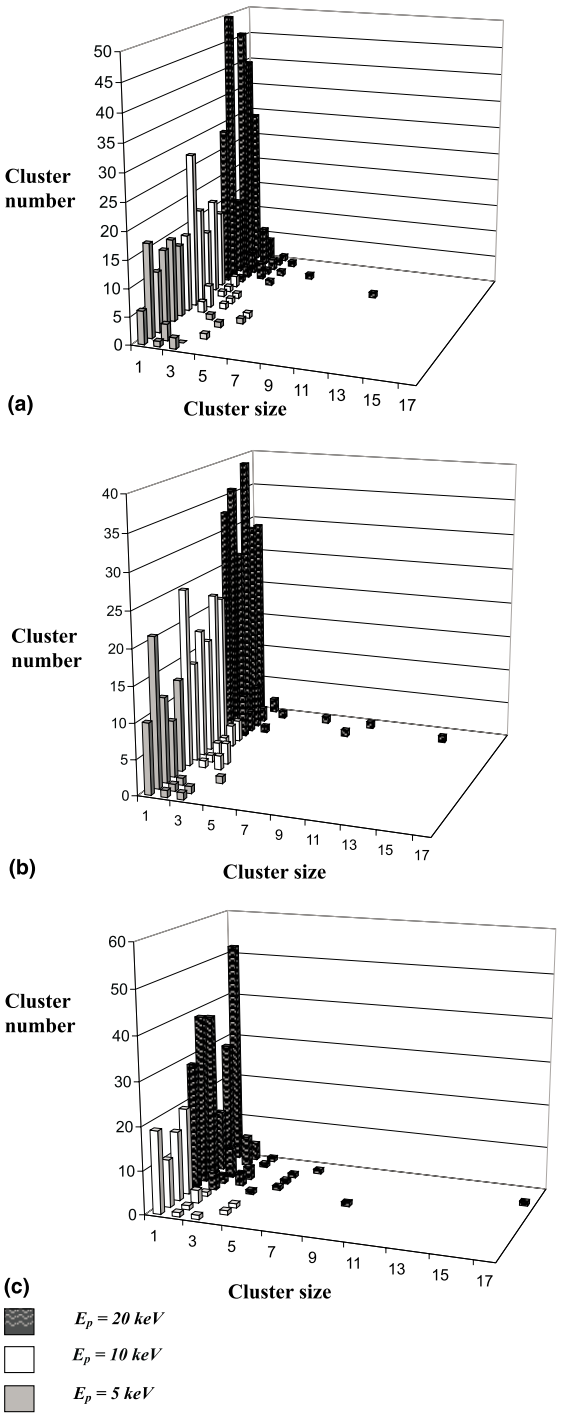

Fig. 8. Size of interstitial clusters in Fe (a), Fe–0.2 at.% Cu (b) and Fe–2 at.% Cu (c) vs PKA energy at 600 K. ■ $E_p = 20$ keV; □ $E_p = 10$ keV; ▨ $E_p = 5$ keV.

in Table 9). For each cascade final configuration, we distributed the corresponding amount of Cu atoms using a random distribution and counted the amount of pairs. Table 9 presents the means on 1000 such computations in order to have statistically converged results. An increase of the number of Cu–V and Cu–I pairs can

Table 9
Mean number of V–Cu and I–Cu pairs created during the cascades

	Mean V (/I) number	Random V–Cu pairs (mean)	Random I–Cu pairs (mean)	V–Cu pairs created (mean)	I–Cu pairs created (mean)
20 keV 0.2 at.% Cu	45.7	0.4	0.5	1.2	0.7
10 keV 0.2 at.% Cu	26	0.4	0.4	0.8	1.2
20 keV 2 at.% Cu	55.3	5.5	4.6	13.5	5.3
10 keV 2 at.% Cu	22.3	2.5	2.4	5.3	3.3

be seen; this is particularly visible for the 2 at.% Cu dilute alloy. The Cu atoms bind more eagerly to the vacancies than to the interstitials, as the increase in the number of Cu–V pairs is more important than that of Cu–I pairs. Calder et al. observed the same phenomenon in 1 at.% Cu [21]. Some mixed objects appear (containing both point defects and Cu atoms) as can be seen in Figs. 9 and 10 as could be expected from the vacancy-mixed objects binding energy displayed in Table 10 (this table displays only the results for the least energetic configurations).

The number of Cu atoms in solution (or isolated Cu atoms, defined in this study as being one Cu atom with eight Fe atoms in the eight first nearest neighbor sites) decreases because of the cascade (specially in the 2 at.% Cu case), and Cu–Cu pairs are created or small Cu clusters originally in the array crystal before the cascade increase in size.

5. Discussion

In the time scale covered by MD simulations, the presence of Cu atoms does not seem to influence in an obvious manner the primary damage (in the limits of the properties examined in this paper). The amount of residual defects is similar and lies in the scattering range of the data, the tendency to form clusters also. Cu atoms have almost the same mass as Fe atoms, that may be one of the reason why no clear influence is observed in the

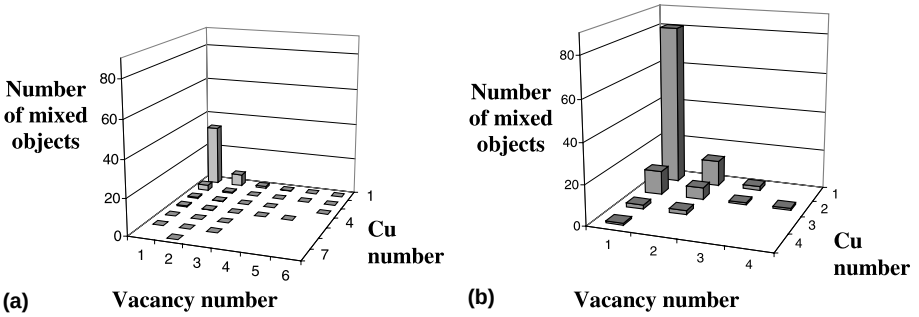

Fig. 9. Distribution of mixed entities containing Cu and vacancies for Fe–2 at.% Cu for 20 keV cascades at 600 K: (a) random distribution; (b) MD results.

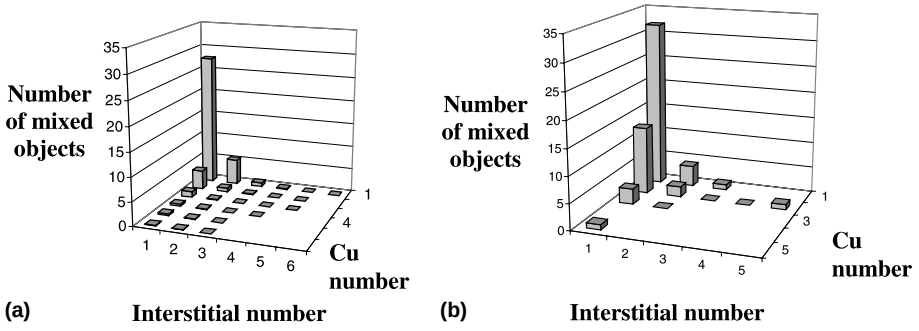

Fig. 10. Distribution of mixed entities containing Cu and interstitials for Fe–2 at.% Cu for 20 keV cascades at 600 K: (a) random distribution; (b) MD results.

Table 10
Binding energy (eV) of one vacancy with a mixed V–Cu defect for different object sizes[a]

Vacancy number	Number of copper atoms					
	0	1	2	3	4	5
0	n.d.	0.192	0.201	0.335	0.292	0.729
1	0.207	0.401	0.537	0.603	0.859	0.484
2	0.359	0.394	0.784	0.384	0.396	n.d.
3	0.631	0.452	0.571	0.482	0.603	n.d.
4	0.629	0.684	0.611	n.d.	n.d.	n.d.
5	0.901	0.573	n.d.	n.d.	n.d.	n.d.
6	0.624	0.674	n.d.	n.d.	n.d.	n.d.
7	0.895	n.d.	n.d.	n.d.	n.d.	n.d.
8	0.622	n.d.	n.d.	n.d.	n.d.	n.d.
9	1.095	n.d.	n.d.	n.d.	n.d.	n.d.

[a] For each size, the most stable configuration was chosen. n.d. = not determined.

course of the MD simulations. MD can only simulate the ballistic processes taking place when a recoil atom is ejected from its lattice position and no diffusion can take place in the time scale covered by MD.

A slight tendency to form small Cu-rich entities has however been observed in this study. This effect is more visible for the 2 at.% Cu alloy. Calder et al. [21] who studied 1 at.% Cu noticed also a slight tendency to form Cu–V pairs. However, neither Cu precipitates, nor dilute atmospheres have been observed to form, while it is known experimentally that dilute solute atmospheres do form under neutron irradiation [6,7] in dilute copper alloys (Cu content lower than 0.2%). It is not possible to directly conclude from this study about the role of displacement cascades on the atmospheres formation, however, because of the very strong binding energies between Cu atoms and vacancies, we expect that the occurrence of many vacancies created by the cascades will affect the Cu atoms. The numerous Cu-rich entities created in the 2 at.% Cu alloy seem to indicate the same trend. This is what has been indeed observed by the kinetic Monte Carlo (KMC) simulations we have performed [66] using as a starting point the results (the residual vacancies) of MD simulations of cascades. These KMC simulations done on the primary damage obtained by MD in Fe–0.2 % Cu alloys have led to the formation of 'mixed clusters' containing both Cu atoms and vacancies and they have shown that the Cu atoms were 'transported' by the numerous vacancies created by the cascades.

The role of interstitials is more difficult to establish. Mixed Cu–I objects do form in the course of the cascade in the 2 at.% Cu alloy, however, some MD simulations done at 300 and 800 K of a single mixed (Cu–Fe) dumbbell in an α-Fe matrix as well as in a 0.2% Cu matrix seem to indicate that Cu atoms are not transported by the dumbbell during its motion [48] at these temperatures. We calculated by ab initio methods [48] the binding energy between one mono-interstitial and a copper atom and found it to be around 0.2 eV. The interstitials may thus play a role in transporting Cu as indicated in Maury's work [67] and more work is in progress to clarify this point. There may be some subtle effects that we have yet to discover, but it will be in any case very difficult to distinguish if these arise from the cohesive model chosen as in [26] or if it is the chemical effect which is responsible. The lack of experimental data on the Fe–Cu system prevents us from making a good assessment of the quality of the potentials to reproduce accurately the Fe–Cu interactions. For instance, these potentials have an isotropic cohesion term; this clearly is an approximation, particularly for transition metals. It would be very interesting to have displacement cascades studied with, for instance, the long range pair potentials derived by Osetsky [22–24]. A better knowledge of the Cu-point defects binding and migration energies is also necessary as small mixed objects seem to play an important role.

Nevertheless, we feel, in the limit of the properties examined in this study, that the potential used here should give reasonable trends of the influence of copper atoms on the displacement cascades.

6. Conclusions

We have performed MD simulations of displacement cascades in α-Fe and in two dilute Cu alloys and analyzed the primary damage for both cases. The presence of a small amount of Cu atoms in Fe matrix does not seem to have any noticeable influence on the damage as defined by the number of residual vacancies, size of the cascades and tendency to form point defect clusters. Neither Cu precipitates, nor dilute atmospheres have been observed to form in the course of the MD simulations. However, a tendency to form small Cu-rich objects (V–Cu or I–Cu pairs for the 0.2 at.% Cu, bigger defects for the 2 at.% Cu) has been noticed. This fact

Table 11
Parameters used for the pair components hardening[a]

Fe: $Z = 26$					
$b_1 = 0.190945$	$c_1 = 2.79686704$	$A_0 = 9.18218708$	$d_0 = 7069.7203$	$B_0 = 43.442150$	$r_1 = 0.305$
$b_2 = 0.473674$	$c_2 = 6.39787954$	$A_1 = 5.65902519$	$d_1 = -4.6$	$B_1 = -75.731567$	$r_2 = 0.620$
$b_3 = 0.335381$	$c_3 = 19.27122561$	$A_2 = -35.5801544$		$B_2 = 48.051086$	$r_3 = 1.300$
		$A_3 = 29.3620796$		$B_3 = -10.61169$	$r_4 = 2.100$
Cu: $Z = 29$					
$b_1 = 0.190945$	$c_1 = 2.90055275$	$A_0 = -9.1998558$	$d_0 = 7069.7203$	$B_0 = 388.914124$	$r_1 = 1.000$
$b_2 = 0.473674$	$c_2 = 6.63506222$	$A_1 = 42.4975433$	$d_1 = -4.5$	$B_1 = -592.499573$	$r_2 = 1.500$
$b_3 = 0.335381$	$c_3 = 19.985651$	$A_2 = -38.5768776$		$B_2 = 303.115295$	$r_3 = 1.900$
		$A_3 = 10.1822491$		$B_3 = -52.0626221$	$r_4 = 2.100$
Fe–Cu					
$b_1 = 0.190945$	$c_1 = 2.8489479087$	$A_0 = 11.8191023866$	–	–	$r_1 = 1.000$
$b_2 = 0.473674$	$c_2 = 6.5170152909$	$A_1 = -11.827953585$	–	–	$r_2 = 2.100$
$b_3 = 0.335381$	$c_3 = 19.6300778985$	$A_2 = 6.74169032899$	–	–	–
		$A_3 = -1.88346082066$	–	–	

[a] $e^2 = 14.4$ eV.

added to recent kinetic Monte Carlo simulation results confirms our feeling that the numerous vacancies left at the end of the cascade recombination phase will interact with the Cu atoms and will act as attractive nuclei. The role of the interstitials is still under investigation.

Appendix A

To be suitable for displacement cascades simulation, it becomes necessary to modify the short range part of the EAM potential because of the energies characteristics of recoil atoms in displacement cascades. For the pair component, one usually uses at short range, potentials such as the 'universal' screened-Coulomb potential of Biersack and coworkers [68]. For intermediate ranges, one typically uses Born Mayer type potentials similar to that published by Maury et al. [61] to give the appropriate threshold displacement energies. Most of the hardening efforts are concentrated on the pair components as the scattering is expected to be dominated by the repulsive part of the potential.

All these functions are joined by smooth interpolation schemes, with coefficients chosen to ensure continuity of the potentials and their first derivative at the knot points.

The electron density and the embedding modification schemes vary from one author to another.

We present below the functions and parameters we used in this work.

A.1. Pair components

Among the pair potentials proposed in [68] we chose that of Wilson et al. [68].

$$
\begin{aligned}
&V(r) = \left(\frac{Z^2e^2}{r}\right)\sum_{i=1}^{3} b_i \exp(-c_i r)\ (\text{eV}),\\
&\quad 0.000 < r < r_1\ (\text{Å}),\\
&V(r) = \exp(A_3r^3 + A_2r^2 + A_1r + A_0)\ (\text{eV}),\\
&\quad r_1 < r < r_2\ (\text{Å}),\\
&V(r) = d_0 \exp(d_1 r)\ (\text{eV}),\\
&\quad r_2 < r < r_3\ (\text{Å}),\\
&V(r) = \exp(B_3r^3 + B_2r^2 + B_1r + B_0)\ (\text{eV}),\\
&\quad r_3 < r < r_4\ (\text{Å}),\\
&V(r) = V_{\text{EAM}}(r)\ (\text{eV}),\\
&\quad r_4 < r < 5.000\ (\text{Å}).
\end{aligned}
$$

The parameters were chosen so as to reproduce the experimental threshold energies for Fe and Cu. For the Fe–Cu interactions, as no experimental data are available, we simply joined the 'universal' screened-Coulomb potential to the equilibrium part (without any Born Mayer intermediate) adjusting the transition function so

Table 12
Parameters used in the density hardening

Fe		
$A = 0.137886166572$	$C_0 = -24.5116272$	$r_1 = 1.800$
	$C_2 = 26.0691414$	$r_2 = 2.000$
	$C_2 = -8.10432529$	
	$C_3 = 0.319591641$	
Cu		
$\rho_{\text{THOMAS–FERMI}}$	$C_0 = 17.3388004$	$r_1 = 0.700$
	$C_1 = -84.7909546$	$r_2 = 1.000$
	$C_2 = 89.1162491$	
	$C_3 = -31.7062187$	

as to obtain threshold displacement energies of a Cu atom in a α-Fe matrix equal to or higher than that of an Fe atom in the α-Fe matrix (Table 11).

A.2. Electron densities

For the Fe component, following Calder and Bacon [31], the electron density takes a constant value A for $r < 1.800$ Å. For Cu, following Pronnecke et al. [69] we joined the density used in the EAM to the Thomas–Fermi form of the electron density of Cu [68]. The parameters are presented Table 12.

$$\rho(r) = A \left(e^-/\mathring{A}^3\right),$$
$$0.000 < r < r_1 \text{ (Fe)},$$
$$\rho(r) = \rho_{\text{THOMAS FERMI}}(r) \left(e^-/\mathring{A}^3\right),$$
$$0.000 < r < r_1 \text{ (Cu)},$$
$$\rho(r) = \exp(C_3 r^3 + C_2 r^2 + C_1 r + C_0) \left(e^-/\mathring{A}^3\right),$$
$$r_1 < r < r_2,$$
$$\rho(r) = \rho_{\text{EAM}}(r) \left(e^-/\mathring{A}^3\right),$$
$$r_2 < r < 5.000 \text{ (Å)}.$$

A.3. The embedding functions

For Fe, the embedding function was linearly extrapolated for high densities

$$F(\rho) = F_{\text{SIMONELLI}}(\rho) \text{ (eV)}, \quad 0.033987505 < \rho < 3.31571225 \left(e^-/\mathring{A}^3\right).$$

For Cu, the embedding function was saturated at high densities

$$F(\rho) = F_{\text{VOTER}} \text{ (eV)},$$
$$0.000 < \rho < 0.6025531 \left(e^-/\mathring{A}^3\right),$$
$$F(\rho) = -2.1814005509492 \text{ (eV)},$$
$$0.6025531 < \rho < 2.13712 \left(e^-/\mathring{A}^3\right).$$

References

[1] J.T. Buswell, C.A. English, M.G. Hetherington, W.J. Phythian, G.D.W. Smith, G.M. Worrall, in: 14th International Symposium on Effects of Radiation on Materials, ASTM STP 1046, Philadelphia, PA, 1987, p. 127.

[2] E.G. Lucas, G.R. Odette, P.M. Mombrozo, J.W. Shekherd, ASTM STP 870 (1985) 900.

[3] J.C. Van Duysen, J. Bourgoin, C. Janot, J.M. Penisson, in: R.E. Stoller, A.S. Kumar, D.S. Gelles (Eds.), 15th International Symposium, ASTM-STP, ASTM, Philadelphia, PA, 1992, p. 117.

[4] S. Miloudi, J.C. Van Duysen, in: Seventh International Symposium on Environmental Degradation of Materials in Nuclear Power Systems–Water Reactor, Breckenridge, CO, 1995, p. 1179.

[5] S. Miloudi, J.C. Van Duysen, B. Remmerie, R.P. May, in: 18th International Symposium on Effects of Radiation on Materials, ASTM STP, 1997, p. 1325.

[6] M. Akamatsu, J.C. Van Duysen, P. Pareige, P. Auger, J. Nucl. Mater. 225 (1995) 192.

[7] P. Auger, P. Pareige, M. Akamatsu, D. Blavette, J. Nucl. Mater. 225 (1995) 225.

[8] M. Akamatsu, X. Li, P. Moser, J.C. Van Duysen, Ann. Chim. France 18 (1987) 287.

[9] G. Simonelli, R. Pasianot, E.J. Savino, Mater. Res. Soc. Symp. Proc. 291 (1993) 567.

[10] M. Ludwig, D. Farkas, D. Pedraza, S. Schmauder, Modell. Simul. Mater. Sci. Eng. 6 (1998) 19.

[11] T. Diaz de la Rubia, R.S. Averback, H. Hsieh, R. Benedek, J. Mater. Res. 4 (1989) 579.

[12] K. Nordlund, R.S. Averback, Phys. Rev. B 56 (1997) 2421.

[13] A.F. Calder, D.J. Bacon, J. Nucl. Mater. 207 (1993) 25.

[14] A.J. Foreman, C.A. English, W.J. Phythian, Philos. Mag. A 66 (1992) 655.

[15] F. Gao, D.J. Bacon, Philos. Mag. A 71 (1995) 43.

[16] H. Zhu, R.S. Averback, M. Natstasi, Philos. Mag. A 71 (1995) 735.

[17] H.F. Deng, D.J. Bacon, Phys. Rev. B 53 (1996) 11376.

[18] D.J. Bacon, T.D. de la Rubia, J. Nucl. Mater. 216 (1994) 275.

[19] W.J. Phythian, R.E. Stoller, A.J.E. Foreman, A.F. Calder, D.J. Bacon, J. Nucl. Mater. 223 (1995) 245.

[20] R.S. Averback, T. Diaz de la Rubia, Solid State Phys. 51 (1998) 281.

[21] A.F. Calder, D.J. Bacon, MRS Proc. 439 (1997) 521.

[22] Yu.N. Osetsky, A.G. Mikhin, A. Serra, J. Nucl. Mater. 212–215 (1994) 236.

[23] Yu.N. Osetsky, A.G. Mikhin, A. Serra, Philos. Mag. A 72 (1995) 361.

[24] Yu.N. Osetsky, A. Serra, Philos. Mag. A 73 (1996) 249.

[25] G.J. Ackland, D.J. Bacon, A.F. Calder, T. Harry, Philos. Mag. A 75 (1997) 713.

[26] C.S. Becquart, C. Domain, A. Legris, J.C. VanDuysen, J. Nucl. Mater 280 (1) (2000) 73.

[27] http://www.ims.uconn.edu/centers/simul/index.htm#xmd.

[28] C.S. Becquart, K.M. Decker, C. Domain, J. Ruste, Y. Souffez, J.C. Turbatte, J.C. Van Duysen, in: Proceedings of the Third International Conference on Computer Simulation of Radiation Effects in Solids (COSIRES 1996), Radiat. Eff. Defects Solids 142 (1997) 9.

[29] J.R. Beeler, G.L. Kulcinski, in: P.C. Gehlen, J.R. Beeler, R.I. Jaffee (Eds.), Interatomic Potentials and Simulation of Lattice Defects, Plenum, New York, 1972, p. 735.

[30] C.H. Bennett, in: A.S. Norwick, J.J. Burton (Eds.), Diffusion in Solids, Recent Developments, Academic Press, New York, 1975, p. 85.

[31] A.F. Calder, D.J. Bacon, J. Nucl. Mater. 207 (1993) 25.

[32] R.E. Stoller, J. Nucl. Mater. 276 (2000) 22.

[33] F. Gao, D.J. Bacon, P.E.J. Flewitt, T.A. Lewis, J. Nucl. Mater. 249 (1997) 77.

[34] R Vascon, doctoral thesis, Université Paris XI, 1997.

[35] M. Hou, Phys. Rev. B 31 (7) (1985) 4178.

[36] M.S. Daw, M.I. Baskes, Phys. Rev. Lett. 50 (1983) 1285.
[37] J.M. Raulot, Master of Science thesis, Université de Marne la vallée, 1998.
[38] D. Farkas, C.G. Schon, M.S.F. de Lima, H. Goldenstein, Acta Mater. 44 (1996) 409.
[39] C. Kittel, Introduction to Solid State Physics, 6th Ed., Wiley, New York, 1987.
[40] J.A. Rayne, B.S. Chandrasekhar, Phys. Rev. B 122 (1961) 1714.
[41] B.N. Brockouse, H. Abou-Helal, E.D. Hallman, Solid State Commun. 5 (1967) 211.
[42] C.J. Smithells, Metals Reference Book, Butterworths, London, 1967.
[43] L.D. Schepper, D. Segers, L. Dorikens-Vanpraet, M. Dorikens, G. Knuyt, L.M. Stals, P. Moser, Phys. Rev. B 27 (1983) 5257.
[44] H.E. Schaefer, K. Maier, M. Weller, D. Herlach, A. Seeger, J. Diehl, Scripta Met. 11 (1977) 803.
[45] A. Vehanen, P. Hautojärvi, J. Johansson, J. Yli-Kauppila, P. Moser, Phys. Rev. B 25 (1982) 762.
[46] L.J. Cuddy, Acta Metall. 16 (1968) 23.
[47] A.F. Voter, Los Alamos Unclassified Technical Report 93-3901, Los Alamos National Laboratory, 1993.
[48] C.S. Becquart, C. Domain, unpublished results.
[49] W.J. Phythian, A.J. Foreman, C.A. English, J.T. Buswell, M. Hetherington, K. Roberts, S. Pizzini, in: R.E. Stoller, A.S. Kumar, D.S. Gelles (Eds.), 15th International Symposium on Effects of Radiation on Materials, ASTM STP 1125, American Society for Testing and Materials, Philadelphia, PA, 1992, p. 131.
[50] T. Kraft, P.M. Markus, M. Methfessel, M. Scheffler, Phys. Rev. B 48 (1993) 5886.
[51] Z.W. Lu, S.H. Wei, A. Zunger, Phys. Rev. B 41 (1990) 2699.
[52] M.H. Mathon, PhD thesis, CEA-5701, ISSN 0429-3460, 1995.
[53] R. Hultgren, P.D. Desai, D.T. Hawkins, M. Gleiser, K.K. Kelley, Selected Values of the Thermodynamic Properties of Binary Alloys, ASM, Metals Park, OH.
[54] G. Brauer, K. Popp, Phys. Stat. Sol. 102 (1987) 79.
[55] K. Masuda, J. Phys. 43 (1982) 921.
[56] A. Weidinger, R. Wessner, T. Wichert, E. Recknagel, Phys. Lett. A 72 (1979) 369.
[57] S. Reintsema, E. Verbiest, J. Odeurs, H. Pattyn, J. Phys. F 9 (1979) 1511.
[58] S.I. Golubov, Yu.N. Osetsky, A. Serra, A.V. Barashev, J. Nucl. Mater. 226 (1995) 252.
[59] X. Li, doctoral thesis, University of Grenoble, 1996.
[60] E.G. Lucas, G.R. Odette, P.M. Mombrozo, J.W. Shekherd, ASTM STP 870 (1985) 900.
[61] F. Maury, M. Biget, P. Vajda, A. Lucasson, P. Lucasson, Phys. Rev. B 14 (1976) 5303.
[62] R.E. Stoller, J. Nucl. Mater. 283–287 (2000) 746.
[63] G. Leibfried, Bestrahlungseffekte in Festkörpern Materialen, Teubner, Stuttgart, 1965.
[64] M.T. Robinson, I. Torrens, Phys. Rev. B 9 (1974) 5008.
[65] D.J. Bacon, F. Gao, A.V. Barashev, Y.N. Osetsky, Mater. Res. Soc. Symp. 540 (1999) 617.
[66] C. Domain, C.S. Becquart, J.C. VanDuysen, MRS Proc. 540 (1999) 643.
[67] F. Maury, A. Lucasson, P. Moser, F. Faudot, J. Phys.: Condens. Matter 2 (1990) 9291.
[68] J. Ziegler, J.P. Biersack, U. Littmark, The Stopping and Range of Ions, vol. 1, Pergamon, New York, 1985.
[69] S. Prönnecke, A. Caro, M. Victoria, T. Diaz de la Rubia, M.W. Guinan, J. Mater. Res. 6 (1991) 483.
[70] H.A. Wriedt, L.S. Darken, Trans. Met. Soc. AIME 218 (1960) 30.